2017 IEEE/RSJ International Conference on Intelligent Robots and Systems (IROS)
September 24–28, 2017, Vancouver, BC, Canada

FLEGX: a bioinspired design for a jumping humanoid leg

Mariapaola D'Imperio[1], Daniele Ludovico[2], Cristiano Pizzamiglio[2], Carlo Canali[1], Darwin Caldwell[1] and Ferdinando Cannella[1]

***Abstract*— Robotics in the last decades is moving towards bioinspired solutions in order to develop systems increasingly integrated with the human environment. Among them, legged robots fascinates more and more researchers thanks to their ability of moving in unstructured environment such as the ones typical of earthquakes, where in the near future robots are planned to be send to help humans while performing dangerous tasks. On the base of this findings, the authors propose a novel concept for a jumping humanoid leg, based on the key role played from the structural flexibility. The geometric and dynamic features of this leg have been selected thanks to a targeted set of numerical simulations. An extensive campaign of experimental tests useful for the validation of the numerical model here presented will be a matter of future works.**

I. INTRODUCTION

Robots are machines designed to assist humans in their daily life or to substitute them while performing heavy or dangerous tasks; for these reasons their shape and functionalities often tend to reproduce systems observed in nature, by designing simpler and more effective solutions from the one characteristic of the natural world, as happens for the bio-inspired robots.

To date several examples belonging to this category, we can cite miniature robots able to fly like a dragonfly [1]; devices that can adapt theirs shape to the surrounding environment one as the octopus [2]; mechanisms that adhere to walls like geckos [3]; legged robots designed to achieve highly efficient locomotion [4] and many others are the biological capabilities modelled for robotics applications.

Nowadays many and many researchers are fascinated by the legged robots development thanks to their ability to move on uneven terrains with respect to wheeled robots.

An optimal design for a legged robot requires the identification of the desired dynamic capabilities and as a consequence of that the actuation system type, the joints characteristics and the structural flexibility level have to be chosen. There are three main pure actuation systems: the electric, the hydraulic and the pneumatic one. The latter is the one that represents better the muscle behaviour: it is composed by a pairs of motors often working in an agonistic-antagonist configuration as happens for the ones so called

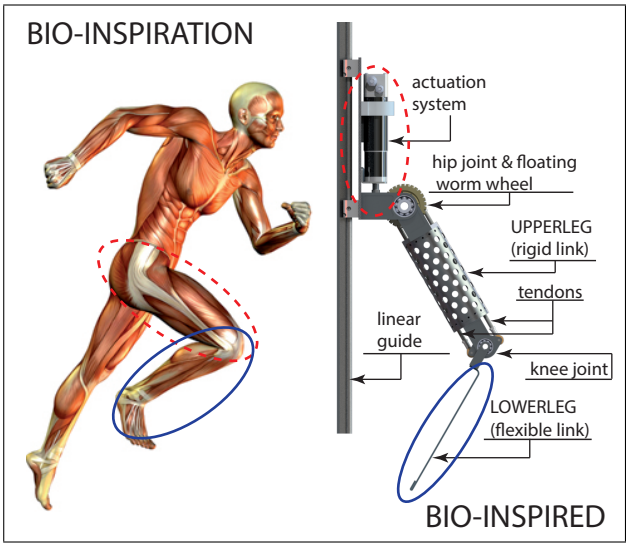

Fig. 1. From the bioinspiration to a bioinspired mechanism. FLEGX components and characteristics.

Pneumatic Artificial Muscles [5], operated by pressurized air in a pneumatic bladder.

Joints and structure, from their side, can be rigid or flexible. The first choice guarantees high task performances precisions but it results in solutions often bulky, massive and not safe for the human interaction. At the opposite, working with flexible connections and structures results in hard to control mechanisms but safe and with a great potential in dynamic performances.

A bio-inspired rigid connection can be found in the MiniHyq knee joint [6]–[8].

The counterexample offered by the Series Elastic Actuator as flexible connections is found in many legged robots. Their design is based on the stiffness reduction thanks to a compliant element placed between the train and the driven load [9]. They can achieve satisfactory performances in force control thanks to the lower friction in the mechanism and, for these reasons, they are well suited for unstructured environments applications.

The family of rigid legged robots includes multiple examples of complex machines having from two legs, in case of humanoids, up to six legs for the exapods and many others [10]. According to the authors opinion, however, it is hard to say that they are truly bio-inspired, since many of them are completely rigid while the structural flexibility plays a key role in many movements typical of the animal world. A classification of biologist researchers, in fact, shows that

[1]Mariapaola D'Imperio, Carlo Canali, Darwin Caldwell and Ferdinando Cannella are with the ADVR, Advanced Robotics Department of Istituto Italiano di Tecnologia, Genoa, Italy. {*mariapaola.dimperio carlo.canali darwin.caldwell ferdinando.cannella*}*@iit.it*

[2]Daniele Ludovico and Cristiano Pizzamiglio are with the DIMEAS, Department of Mechanical and Aerospace Engineering at Politecnico di Torino, Turin, Italy. daniele.ludovico@studenti.polito.it, cristiano.pizzamiglio@polito.it

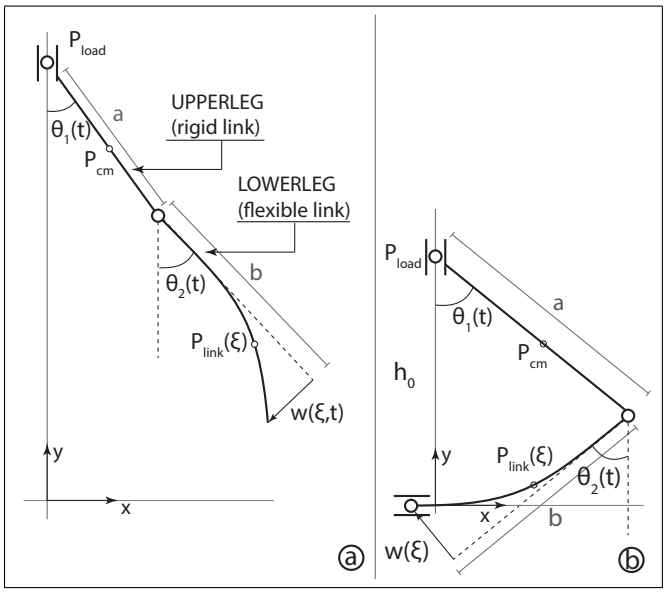

Fig. 2. FLEGX kinematics: a) stance phase; b) landing phase.

many locomotion movements depend on elastic mechanisms: walking, running and modest jumps rely on energy conservation; standing jumps are based on energy amplification while energy absorption is the core of landing movements [11].

On the base of this findings, the authors decided to investigate the performance of a jumping humanoid robotic leg having one structural component conceived as flexible. It is called FLEGX (FLEXible LEG) and its geometric and dynamic features have been selected thanks to a targeted campaign of numerical simulations. The settings and results of these analysis, performed using the software MSC.Nastran® and MSC.Adams®-Matlab/Simulink® integrated environment, will be described below.

The rest of the paper is organized as follows. In Section II FLEGX mechanism is described while the different multibody models developed to test the leg performances are detailed in Section III; Section IV analyses the dynamic simulations and at the end Section V addresses results and conclusions.

II. Mechanism Description

The novel robotic leg described in this paper is called FLEGX and it is characterized mainly for having one structural component conceived as flexible (Fig. 1). Its design derives from an extended optimization campaign focused on two objectives: lowering both masses and inertias and, at the same time, increasing the dynamic capabilities of the system, i.e. the jumping height. The leg has 3DoF in the sagittal plane: the two rotational movements (hip joint - θ_1, Fig. 2.a - and knee joint - θ_2, Fig. 2.a) are actuated, and, their configurations constraint the position of the third degree of freedom, the translational one (y direction in Fig. 2.a).

The reduction of masses and inertias was achieved by locating the actuation system, composed by two brushless DC motors with two gearheads, on the linear guide supporting plate (Fig. 1) and not directly on the leg structure. In order to transmit the motion at the knee joint, then, a floating worm wheel and a tendon-like structure (Fig. 1) is employed. The second source of weight reduction can be found in the upperleg design, since the tube that composes this part is featured with several holes (Fig. 1).

The rise of the dynamic capabilities of such leg depends on the lower leg design (Fig. 1): it consists in a flexible spring steel (AISI 304 - EN 1.4301) link having constant rectangular cross-section. Several details of this component will be exhaustively illustrated in the rest of the paper.

III. Multibody Models

Two different multibody models have been developed to analyse the robotic leg performances: one of them, the so called Machinery Model (MM), was more focused on mechanical aspects such as the flexible link modelling, while the other one, named Cosimulated Machinery Model (CSM), mainly concerns control aspects. In all of the aforementioned models, using the MSC.Adams/Machinery® module, a detailed virtual prototype of the motion transmission system was implemented with the aim of assessing the influence of the worm gear efficiency on the overall performance of the FLEGX robotic limb.

A. Machinery Model

An extensive numerical simulation campaign was performed, using the software MSC.Adams®, with the aim of studying the dynamics of a countermovement jump. At first, the take-off and landing phases were investigated separately in order to understand how to tackle the issues associated with them, for instance, the definition of suitable motion laws or of optimal solver parameters. Then, these two stages of the jump were merged together and a complete simulation of a countermovement jump was achieved.
Two different modelling options for the flexible lower link were evaluated and the corresponding results were compared:

- Linear flexible link, based on modal flexibility.
- Nonlinear flexible link, based on implicit nonlinear finite element analysis.

1) Linear flexible link: The flexible component, in this model, has been modelled as a simplified Finite Element Model containing only the mode-shape required for a dynamic description of the system according to the Craig-Bampton orthonormalization procedure [12]. Following this theory, the system displacements u can be boundary (u_B) or interior (u_I). The first one are obtained by giving to each of them a unit displacement and keeping all the others fixed; the seconds instead, are calculated by fixing the u_B and computing an eigensolution. At the end, the relationship obtained is given by

$$u = \begin{bmatrix} u_B \\ u_I \end{bmatrix} = \begin{bmatrix} I, 0 \\ \Phi_{IC}, \Phi_{IN} \end{bmatrix} \begin{bmatrix} q_C \\ q_N \end{bmatrix} \quad (1)$$

where Φ_{IC} represents the physical displacement of the u_I, Φ_{IN} are the physical displacement of the normal modes, q_C are the modal coordinates of the constraint modes while

q_N are the modal coordinates of the fixed-boundary normal modes.

Thanks to this substitution is then possible to rewrite the system stiffness matrix ($\hat{K}$) as a block diagonal due to the absence of coupling effects between the constraints modes and the fixed boundary ones

$$\hat{K} = \Phi^T K \Phi = \begin{bmatrix} I, 0 \\ \Phi_{IC}, \Phi_{IN} \end{bmatrix}^T \begin{bmatrix} K_{BB}, K_{BI} \\ K_{IB}, K_{II} \end{bmatrix} \begin{bmatrix} I, 0 \\ \Phi_{IC}, \Phi_{IN} \end{bmatrix} = \begin{bmatrix} \hat{K}_{CC}, 0 \\ 0, \hat{K}_{NN} \end{bmatrix} \tag{2}$$

At the opposite, instead, the mass matrix ($\hat{M}$) is not block diagonal because of the inertia coupling effects between the constraint modes and the fixed-boundary ones.

$$\hat{M} = \Phi^T M \Phi = \begin{bmatrix} \hat{M}_{CC}, \hat{M}_{NC} \\ \hat{M}_{CN}, \hat{M}_{NN} \end{bmatrix} \tag{3}$$

2) Nonlinear flexible link: The nonlinear flexible model of the lower leg was built using the MSC.Adams/MaxFlex® module. As stated in [13], MSC.Adams/MaxFlex® converts the equation of motion in nonlinear finite element (FE) domain into phase-state form and discretizes them in time according to the multibody system (MBS) integrator settings. The data exchanges between the MBS and FE domain and the control of solution flow are implemented in a Simulation Component Architecture (SCA) framework with the nonlinear FE solver implemented as a Non-Linear Finite Element (NLFE) service.

In contrast to the linear flexible model based on the modal neutral file, the nonlinear modelling technique is based on a run-ready data deck suitable for MSC.Nastran® implicit nonlinear analysis (SOL400). The mesh of the component was defined via the bulk data file (BDF); the BDF was imported in MSC.Adams® GUI and then at analysis time the GUI generates the run-ready data deck to be used in the analysis; also for the nonlinear model of the lower link, the mesh was built using two-dimensional quadrilateral CQUAD4 elements [14]. One of the potential of the MSC.Adams/MaxFlex® module lies in the possibility of representing geometric nonlinearities, such as large deformations; indeed, with the linear modelling option is possible to get reliable results only if the component undergoes deformations that are approximately less than 10% of the characteristic length of the component.

Eventually, it is easy to understand that the simulations performed including a nonlinear component in the multibody model feature a much higher computational cost with respect to the ones carried out with a linear flexible link. The nonlinear simulations described below were run on a machine with an Intel® Core™ i7-4800MQ processor (2.70GHz) and with 16GB RAM.

B. Cosimulated Machinery Model

The control algorithm, implemented in the Cosimulated Machinery Model, was studied in the MSC.Adams®-Matlab/Simulink® integrated environment: the first software solves the system dynamics dealing with FLEGX multibody model, considering the linear flexible link model and including the effect of the gear system; while the second one allows to implement and test the control scheme.

The control algorithm is based on the assumed mode Lagrangian dynamic model of the system. According to the hybrid system theory [15], the dynamic of the mechanism is divided in the two different phases. In the flying phase (Fig. 2.a) since the actuators and the linear guide supported plate are heavier than the other components of the leg, the motion of the plate is similar to the projectile one. For these reason it is possible to consider the vertical displacement of the leg as an independent variable and the equations which describe the motion of the leg are similar to the equation of a two DOF robotic arm. In the stance phase, intead, the leg stand on the ground (Fig. 2.b).

To control this hybrid system is then necessary to define the switching condition, which in this case is the distance between the leg and the ground, and then to use two different control law, one for each phase.

Starting from the equations of motion of each phase defined as:

$$M(q,\delta)\,\ddot{q} + h\left(q, \dot{q}, \delta, \dot{\delta}\right) + D\left(\dot{q}, \dot{\delta}\right) + G(q,\delta) = \tau \tag{4}$$

it is possible to linearise and then stabilize the system using the following control law:

$$\tau = \tilde{M}(q,\delta)\left(\ddot{q}_{ref} + K_D\left(\dot{q}_{ref} - \dot{q}\right) + K_P\left(q_{ref} - q\right)\right) + \tilde{h}\left(q, \dot{q}, \delta, \dot{\delta}\right) + \tilde{D}\left(\dot{q}\right) + \tilde{G}(q,\delta) \tag{5}$$

where $\tilde{M}(q,\delta)$ is an approximation of the inertia matrix, $\tilde{h}\left(q, \dot{q}, \delta, \dot{\delta}\right)$ resumes the Coriolis effects and centrifugal forces,$\tilde{D}\left(\dot{q}\right)$ contain friction contribution and $\tilde{G}(q,\delta)$ is the gravity compensator.

In this control algorithm the nonlinear static friction model is used. This model also includes Coulumb and viscous effect: $\tilde{D}\left(\dot{q}\right) = F_c sgn\left(\dot{q}\right) + \beta\dot{q}$.

C. Worm gear virtual prototype

As stated above, FLEGX system features a couple of right-hand worm gear sets. Worm gears efficiency, which typically ranges between 0.40 and 0.85, depends on various factors, for instance, the lead angle, the gear ratio, the running speed and the lubrication conditions. The efficiency can be computed in the following way (worm driving) [16]:

$$\eta = \frac{\cos\vartheta_n - f\tan\alpha}{\cos\vartheta_n + (f/\tan\alpha)} \tag{6}$$

where f is the friction coefficient of the materials in contact, α is the worm lead angle and θ_n is the normal pressure angle given by

$$\tan\vartheta_n = \tan\vartheta\cos\alpha. \tag{7}$$

It is clear that the efficiency of the worm gears can significantly affect the overall performance of the robotic leg, thus a detailed study is needed.

Virtual prototypes of the worm gears were implemented, in the FLEGX multibody model, using the MSC.Adams/Machinery® module. The 3D Contact algorithm was employed: it uses a geometry-based contact and is able to compute true backlash based on actual working center distance and tooth thickness [17].

Both worm gear sets are identical. The pressure angle is equal to $15°$, the module is 2.5 and the center distance is equal to 53 mm. The worms, made of case hardened steel, have three threads, while the worm wheels, which feature 29 teeth, are made of bronze (CuZn40Al2/So). If mineral grease is used as lubricant, worm wheels can bear an output torque equal to 77 Nm.

It was very hard to determine realistic contact parameters for the worm gears; as a matter of fact, there is a lack of information in the literature for parameters like the stiffness or the dynamic friction transition velocity. Thus, several simulations were carried out in order to understand how a variation of these parameters could affect the overall behaviour of the system; however, a certain level of uncertainty still remained for the values of the damping coefficient, the static and dynamic friction transition velocities. The value of the static friction coefficient μ_s was determined in accordance with the information provided by the worm gear manufacturer: for the worm gear chosen, an efficiency equal to 0.64 was declared. However, considering that the starting efficiency is lower than the running efficiency and many other factors can reduce the efficiency of the worm gear, such as the sliding velocity and the temperature, a 0.60 efficiency was assumed. By using Eq. 6, the corresponding friction coefficient can be evaluated and it is approximately equal to 0.14; the dynamic static coefficient was then set equal to 0.13.

IV. Multibody Dynamics Simulations

The dynamic simulations of the MM were performed by giving in input at each joint a desired angular motion law, while in the CMM the movements derive from a proper control algorithm as detailed in the rest of this paragraph.

A. Machinery Model Analysis

The simulations carried out with the MM, as stated above, were focused on the analysis of the system mechanical performances. For the numerical analyses of the counter-movement jump, the virtual model of the FLEGX mechanism was equipped with two different link geometries; both the links are 250 mm long and 70 mm wide, but feature two different thicknesses: 2 mm and 3 mm respectively. In this way, it was possible to evaluate how the stresses and transversal displacement of the flexible link as well as the torques of the brushless DC motors vary in relation to the lower link thickness.

The take-off and landing phases were performed by rotating the hip and the knee joints with proper motion laws as a function of time. The jumping technique can be described as follows: the robotic leg starts at a static standing position and then squats down, in 3 seconds, by a 55 degrees clockwise and counterclockwise rotation, with respect to the vertical axis, of the hip and knee joints respectively; eventually, at $t = 3s$ the hip and knee joints rapidly rotate again, but in the opposite directions, allowing the leg to jump and reaching a 50mm jumping height. When the maximum height of the jump is reached, that is when the center of mass of the robotic limb is temporarily at rest, the descent phase begins; during this phase, with the aim of reducing the high value of the ground reaction force that will occur at the instant of landing, a 30-35 degrees clockwise and counterclockwise rotation of the hip and knee joints respectively is performed. After the instant of landing, the ground reaction force reduces its value and become equal to FLEGX weight. Lastly, the robotic link returns to the initial static standing position at $t = 4s$.

In order to avoid unwanted vibrations, the motions were described by a cubic polynomial function that approximates the Heaviside step function [22], such as:

$$STEP = \begin{cases} \theta_0 : t \leq t_0 \\ \theta_0 - a\Delta^2(3 - 2\Delta) : t_0 < t \leq t_1 \\ \theta_1 : t \geq t_1 \end{cases} \tag{8}$$

with $a = (\theta_1 - \theta_0)$ and $\Delta = \frac{(t-t_0)}{(t_1-t_0)}$.

With the aim of reducing the solution time and avoiding solver issues during the simulations, the contact between the flexible link and the ground was not directly modeled, but the interaction between the ground and a low mass rigid cylinder, constrained by a fixed joint to the lower interface node of the flexible link, was implemented. The contact between the two rigid bodies was modeled using the Impact-Function-Based contact algorithm, which models the contact force as a nonlinear spring damper.

All the simulations were run using the the Hilber-Hughes-Taylor (HHT) integrator. As stated in [17], the HHT solver seems to offer the highest performance and stability, with respect to the GSTIFF integrator, when the Machinery module is used. The default error tolerance, equal to $1 \cdot 10^{-5}$ was not modified.

B. Cosimulated Machinery Model analysis

The simulations carried out with the CMM have the purpose of investigating the control algorithm details, for these reasons they have been performed using the linear model of the flexible link 250 mm long, 70 mm wide and 3 mm thick. To reduce the vibration induced by the actuators the motion law chosen to perform the jump, follows a sinusoidal acceleration profile. In particular starting from the standing position the hip rotates of $55deg$ and knee of $-55deg$ in $0.5sec$, then they return in the standing position in $0.48sec$. Once the leg reaches the maximum height the hip and knee joints rotate of $30deg$ and $-30deg$ in order to reduce the forces due to the impact with the ground.

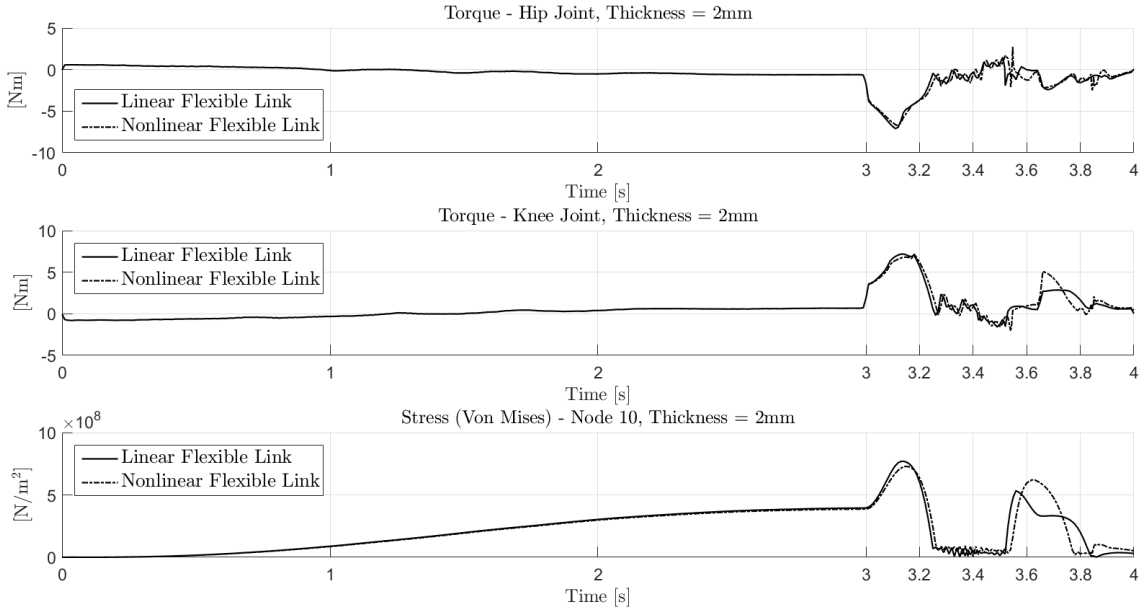

Fig. 3. Take-off and landing analysis. The virtual prototype of the FLEGX robotic limb was equipped with a 250mm long, 70mm wide and 2mm thick flexible link. Comparison of the results obtained with the linear and nonlinear model of the flexible link.

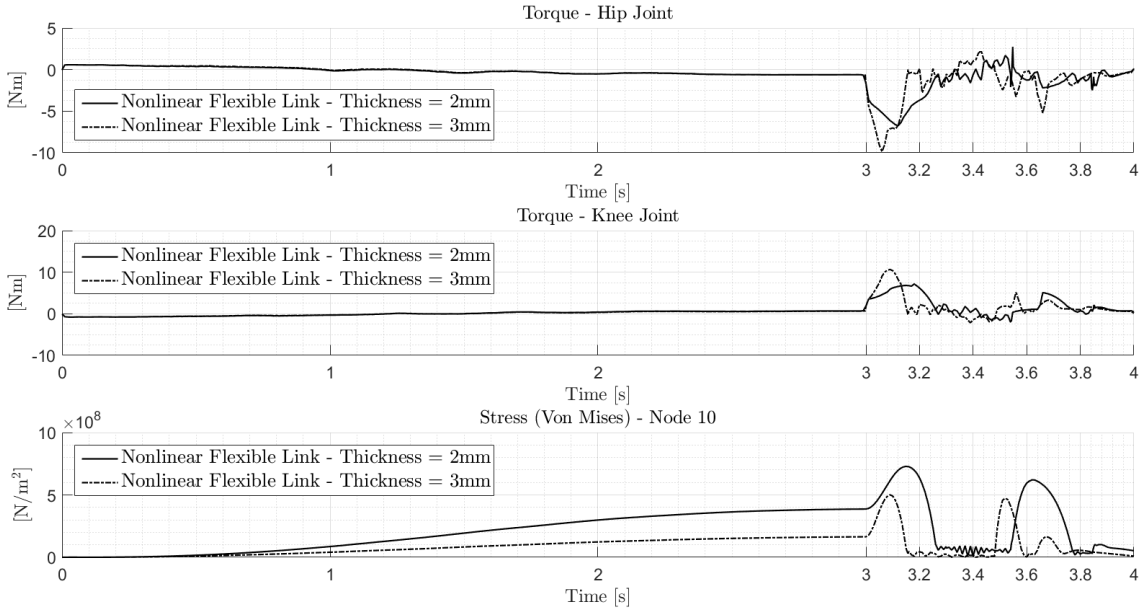

Fig. 4. Study on the effects of the thickness of the link on the FLEGX performance. A take-off, with a maximum jumping height imposed equal to 50mm, and landing analysis was carried out. Two thicknesses for the links were chosen, namely 2 mm and 3 mm and the nonlinear model of the flexible link was employed. The static friction coefficient of the worm gears was set equal to 0.14.

V. Results and Conclusions

In Fig. 3 and Fig. 4 the stresses in the flexible links and the hip and knee torques required during the take-off and landing stages of the jump for the two link thicknesses are shown. For reasons of space, the results of MM simulation for the 3 mm thickness are not reported here because they are summarized somehow in Fig. 4. Moreover, the results obtained with the linear and nonlinear flexible model of the links are compared and, as it can be noticed in Fig. 3, the differences are negligible. Thus, future simulations of the same kind can be performed using the faster modal flexibility technique hence reducing the computational time. In Fig. 3,

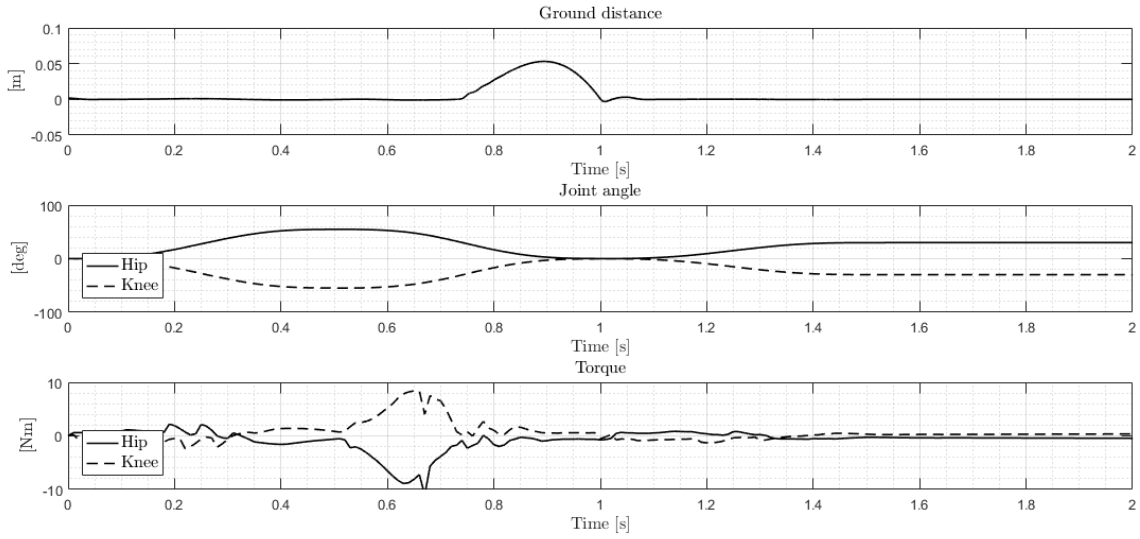

Fig. 5. Results of the cosimulation

at last, it can be observed that with the 2 mm thick flexible link the torques required at the hip and knee joints are smaller with respect those required with the 3 mm thick flexible link; indeed, for the latter the maximum torques (absolute values) at the hip and knee worm are equal to 9.87 Nm and 10.64 Nm respectively, whereas, for the 2 mm thick link, are equal to 6.72 Nm and 7.17 Nm respectively. However, during the instant of take-off, the 2 mm thick flexible link is subjected to a very high stress, at the fixed end of the link, approximately equal to 728 MPa; thus the link is likely to experience plastic deformation.

In Fig. 5 there are the result of the CMM. The jump heigth reached with this motion is of $53mm$. Comparing the result of this cosimulation with the ones done in a previous work where the effect of the gears were not taken into account, it is possible to observe that the torque needed to perform the same type of jump is greater when the gear system is added in the model, then the control law is no more able to damp the oscillation of the flexible link due to the fact that the worm gear does not allow the retrograde motion, and because the friction model used in the control law is not enough accurate. In future it will be necessary to study a more precise model of the friction due to the worm gear in order to allow to damp the oscillation of the leg and increase the performance of the system in terms of trajectory tracking. Future works will be also focused on an extensive campaign of experimental tests carried out with the physical prototype with the aim of collecting data useful for the numerical model validation.

REFERENCES

[1] R. Bogue, "Recent developments in miniature flying robots," *Industrial Robot: An International Journal*, vol. 37, no. 1, pp. 17–22, 2010.

[2] M. Cianchetti, M. Calisti, L. Margheri, M. Kuba, and C. Laschi, "Bioinspired locomotion and grasping in water: the soft eight-arm octopus robot," *Bioinspiration & biomimetics*, vol. 10, no. 3, p. 035003, 2015.

[3] Z. Yu, Z. Wang, R. Liu, P. Wang, and Z. Dai, "Stable gait planning for a gecko-inspired robot to climb on vertical surface," in *Mechatronics and Automation (ICMA), 2013 IEEE International Conference on*. IEEE, 2013, pp. 307–311.

[4] D. W. Haldane, M. Plecnik, J. Yim, and R. Fearing, "Robotic vertical jumping agility via series-elastic power modulation," *Science Robotics*, vol. 1, no. 1, p. eaag2048, 2016.

[5] D. Rus and M. T. Tolley, "Design, fabrication and control of soft robots," *Nature*, vol. 521, no. 7553, pp. 467–475, 2015.

[6] H. Khan, C. Semini, D. Caldwell, and V. Barasuol, "Actuator sizing for highly-dynamic quadruped robots based on squat jumps and running trots," in *Int. Conf. on Climbing and Walking Robots (CLAWAR)*, 2013.

[7] S. Seok, A. Wang, M. Y. Chuah, D. Otten, J. Lang, and S. Kim, "Design principles for highly efficient quadrupeds and implementation on the mit cheetah robot," in *Robotics and Automation (ICRA), 2013 IEEE International Conference on*. IEEE, 2013, pp. 3307–3312.

[8] M. Faschingbauer, H. J. Heuer, K. Seide, R. Wendlandt, M. Münch, C. Jürgens, and R. Kirchner, "Accuracy of a hexapod parallel robot kinematics based external fixator," *The International Journal of Medical Robotics and Computer Assisted Surgery*, vol. 11, no. 4, pp. 424–435, 2015.

[9] J. E. Pratt and B. T. Krupp, "Series elastic actuators for legged robots," in *Defense and Security*. International Society for Optics and Photonics, 2004, pp. 135–144.

[10] I.-W. Park, J.-Y. Kim, J. Lee, and J.-H. Oh, "Mechanical design of humanoid robot platform khr-3 (kaist humanoid robot 3: Hubo)," in *Humanoid Robots, 2005 5th IEEE-RAS International Conference on*. IEEE, 2005, pp. 321–326.

[11] Y. Bar-Cohen and C. Breazeal, "Biologically inspired intelligent robots," in *Smart Structures and Materials*. International Society for Optics and Photonics, 2003, pp. 14–20.

[12] J.-G. Kim and P.-S. Lee, "An enhanced craig–bampton method," *International Journal for Numerical Methods in Engineering*, vol. 103, no. 2, pp. 79–93, 2015.

[13] M. Software, "Welcome to adams maxflex," D, Tech. Rep., 2017.

[14] M. Nastran, "Quick reference guide, msc," *Software Corporation*, 2001.

[15] J. Kostamo, M. Focchi, E. Guglielmino, J. Kostamo, C. Semini, J. Buchli, M. Pietola, and D. Caldwell, "A magnetorheologically damped compliant foot for a legged robotic application," *Journal of mechanical design*, p. 136, 2013.

[16] G.Jacazio and S.Pastorelli, *Meccanica Applicata alle Macchine*. Levrotto&Bella, Torino, 2001.

[17] M. Software, "Welcome to adams machinery," D, Tech. Rep., 2017.